Preprints of the 21st IFAC World Congress (Virtual)
Berlin, Germany, July 12-17, 2020

Hysteresis Dispersion Compensation with Neural Network based Controller

L.Amigues * **V.Pommier-Budinger** * **J.Bordeneuve** *

* *ISAE-SUPAERO, Université de Toulouse, 31400 Toulouse, France (e-mail: louis.amigues@isae-supaero.fr valerie.budinger@isae-supaero.fr joel.bordeneuve@isae-supaero.fr).*

Abstract: Hysteresis is a commonly encountered physical phenomenon in many systems. It results in a dependence of the state of a system to its history. This non-linearity makes it particularly difficult to control accurately. There are many ways for compensating hysteresis, one of them consists of building an inverse model of the hysteresis and using it as a feedforward controller. Coupled to a feedback mechanism, the hysteresis impact can thus be minimized. However, the performance of these controllers decreases when exposed to dispersion in the hysteresis quantity or shape. The capacity of neural networks to model non-linear phenomena is not to be proven and will be put at use. In this paper, an artificial neural network model was trained to replace the conventional hysteresis inverse model. The controller performance was evaluated on a limited-angle torque motor, which exhibits hysteresis due to the magnetization saturation of the ferromagnetic materials. The experimental results pointed out the superior robustness to system dispersion of the Neural Network based controller for time and frequency response.

Keywords: Hysteresis Compensation, Neural Network, Dispersion Robustness, Hardware In the Loop, Limited-Angle Torque Motor.

1. INTRODUCTION

Hysteresis is a non-linear phenomenon present in diverse fields such as structural mechanics, aerodynamics, electromagnetics... For a single input, a hysteretic system can have many outputs depending on the history of the input. This phenomenon is particularly problematic when controlling systems with accuracy requirement.
Dispersion in the hysteresis quantity would have as consequences a wider or finer hysteresis envelop, and also possibly a different shape. Systems from a same product line can exhibit strong variability in their behavior due to many parameters such as aging, materials imperfections, manufacturing tolerance (Ramarotafika et al., 2013)... The designed controller shall be robust to this dispersion.
The system under study is a Limited Angle Torque Motor (LATM), whose structure is similar to direct current brushless motors (Nasiri-Zarandi et al., 2015) but with its shaft having a small and limited angular displacement range. With no external excitation, the flux produced by the pair of permanent magnets produces a magnetic bridge that stabilizes the rotor in a certain angular position. By applying current to the LATM, its armature windings produces a flux that perturbs the magnetic bridge, thus, the system rotates to a new equilibrium position (Yu and Wang, 2014). Although these systems provide accurate positioning capabilities (Tsai et al., 2009), they exhibit hysteresis due to the saturation of the ferromagnetic material in the armature windings (Tebble and Craik, 1969).
One common way of compensating hysteresis is computing a hysteresis model, being then inverted and used as a feedforward controller. A variety of different models can be used (Hassani et al., 2014), the most commonly encountered are mathematical models such as Prandtl-Ishlinskii (Yi et al., 2019), Preisach (Joey et al., 2019) or Bouc-Wen (Zhou et al., 2019) and physics-based models like Jiles-Atherton (Chen et al., 2019).
Amongst the previously stated models, the Jiles-Atherton model gave the best results for our study case as it describes the hysteresis behavior of the magnetization process of ferromagnetic materials. Many global optimization algorithms are available to identify the best Jiles-Atherton parameters : evolutionary algorithm, Particle Swarm Optimization (Li and Gong, 2019) or its modified version to avoid premature convergence (Chen et al., 2019), genetic algorithms (Lu et al., 2015) or even chaotic optimization methods (Rubežić et al., 2018). However, when exposed to system variability, the performance of the control based on this model decreases (Ramarotafika et al., 2013).
Neural Networks have shown great capacities for modelling nonlinear and multi-valued mapping problems such as hysteresis (Tan et al., 2019; Liang et al., 2019) but also for processing robustness to system variability (Querlioz et al., 2013; Patel et al., 2011). Moreover, by inverting the system input and output during the training process, Neural Networks have great capacities in modelling inverse models (Zhang et al., 2018).
Two control strategies will be assessed in this work to control the hysteresis of a highly dispersed system. Two inverse models, Jiles-Atherton and Neural Network integrated in a control scheme will be used to evaluate the controller robustness in presence of system variability.

2. EXPERIMENTAL SETUP

The torque motor under study is mounted on an experimental test bench to identify and characterize its hysteresis in a first time, and then to apply closed-loop control with Hardware In the Loop (HIL) testing. The experimental setup, Fig 1, of this test bench and the obtained experimental data from the system are described in this section.

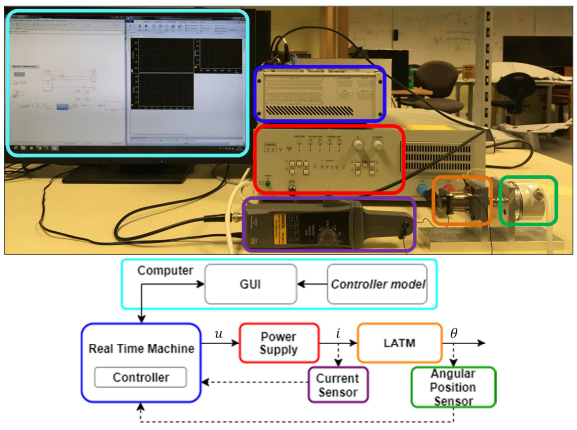

Fig. 1. Experimental test bench : Photography and functionnal diagram

2.1 Test Bench Presentation

Plant The plant is a LATM, which can be described as an electromechanical actuator whose control variable is the input current and the controlled variable is the shaft limited angular position. These motors exhibit hysteresis due to the magnetization saturation of the ferromagnetic materials.

Controller The controller is embedded in a Real Time Machine (RTM). The RTM gathers data from the sensors and provides the power supply unit with the command voltage. The sampling rate is set to 0.1 ms.

Power Supply The power supply is a current amplifier, which transforms the command voltage from the RTM to the corresponding current command. The adjustable cut-off frequency is set to 10 kHz.

Sensors The input, the current, and the output, the angular position, of the hysteretic system are monitored. Both sensors have a bandwidth far greater than the LATM.

- A current clamp is used for the measurement of the current applied to the LATM armature windings.
- A rotary incremental encoder is used for the measurement of the angular position of the LATM shaft. The selected incremental encoder is 6,000 counts per revolution which corresponds to a angular resolution of 0.06° . The sensor is mounted to the test bed with the LATM and are assembled by a bellow coupling to avoid axial misalignment.

2.2 Experimental Characterization

The frequency range of this study is limited to $[0-10]$ Hz. In this frequency domain, the system can be considered rate-independent and following Al Janaideh et al. (2009), the influence of a triangular or harmonic signal for the characterization is neglected.
To characterize the system's hysteresis, the LATM is open-loop controlled with a 1 Hz sinusoidal signal. The magnitude of the signal varies up to the motor's maximum current range, see Fig 2. Each magnitude is maintained for five periods to avoid outliers.

As said in the introduction, the objective is to control hysteresis of systems exhibiting dispersion. For our experiment, only one motor is available, thus, the dispersion must be emulated.
To emulate hysteresis dispersion in the system, a backlash mathematical function is placed between the current command signal and the LATM. The backlash width emulates the hysteresis dispersion by enlarging the hysteresis envelop and reducing the height as the backlash reduces the maximum current output, see Fig 2. The dispersion range for the study has been set to $[0-50]$ mA.

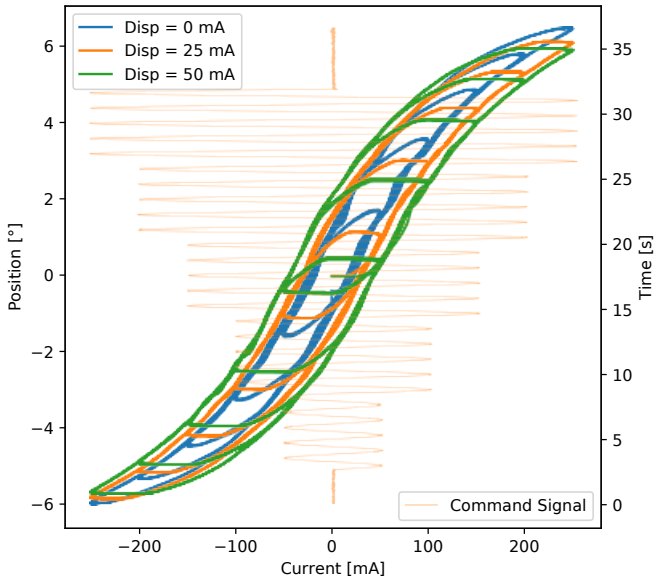

Fig. 2. LATM hysteresis experimental data with emulated dispersion

The characterization of the dispersed system was performed for the whole range with a 5 mA step, 11 data files were obtained and 3 of them are displayed in Fig 2.

A 50% dispersion in the dynamics of the system would also be interesting to study. As the dynamic of our LATM is fixed, the proportional gain of the controller will be modulated, $0.5K_P$ and $1.5K_P$, to emulate this system dynamic dispersion.

3. CONTROLLER DESIGN

The chosen architecture of the controller C is a Proportional Integral (PI) feedback with Anti Wind-up (AW) in parallel of a feedfoward inverse model of the hysteresis $\hat{H}^{-1}$, see Fig 3, which is either the Jiles-Atherton inverse model or the Neural Network inverse model.

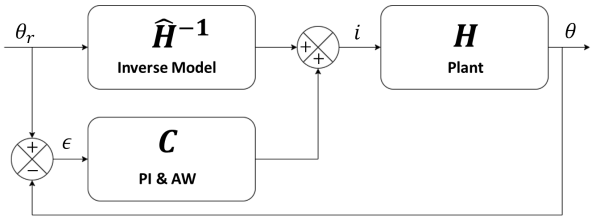

Fig. 3. Designed controller architecture

The equivalent transfer function of the designed controller is given Eq 1.

$$TF = \frac{\theta}{\theta_r} = 1 - \frac{\Delta H}{CH\hat{H} + \hat{H}} \tag{1}$$

With $\Delta H = \hat{H} - H$.
The control compensates the remaining error between the hysteresis model $\hat{H}$ and the plant H.

3.1 Controller Gains

To determine the proportional gain K_P and the integral gain K_I, an iterative process is implemented. The temporal response to a step at different operating points of the system will be analyzed when varying the controller gains. The final set of parameters shall minimize the Integral of Time-weighted Absolute Error (ITAE) performance index which penalizes errors occurring later in the response while minimizing the initial error.
Through the iterative process, the best gains that minimize the ITAE are $K_P = 20$, $K_I = 3500$. These gains will be used for the above control schemes with both inverse models.

3.2 Jiles-Atherton Inverse Models

The Jiles-Atherton model is a widely used physics based model that describes the hysteretic magnetization process of ferromagnetic materials when submitted to a magnetic field (Jiles and Atherton, 1986). The direct model is based on the following equations (Jiles, 2015) :

$$\theta = B + \Delta \tag{2a}$$
$$B = \mu_0(H + M) \tag{2b}$$
$$H = k_i i \tag{2c}$$
$$\frac{\partial M}{\partial H} = \frac{\eta}{(k\delta - \alpha\eta)} \tag{2d}$$
$$\eta = M_{an} - M + kc\delta\frac{\partial M_{an}}{\partial H_e} \tag{2e}$$
$$M_{an} = M_s\left(\coth\left(\frac{H_e}{a}\right) - \frac{a}{H_e}\right) \tag{2f}$$
$$\frac{\partial M_{an}}{\partial H_e} = \frac{M_s}{a}\left(1 - \coth^2\left(\frac{H_e}{a}\right) + \left(\frac{a}{H_e}\right)^2\right) \tag{2g}$$
$$H_e = H + \alpha M \tag{2h}$$
$$\delta = \begin{cases} +1 \text{ if } dH/dt > 0 \\ -1 \text{ if } dH/dt < 0 \end{cases} \tag{2i}$$

The permeability of the medium μ_0, the energy loss constant k, the mean field α, the reversibility factor c, the anhysteretic magnetization shape factor a, the magnetization saturation M_s, the current gain k_i and the position offset Δ are the eight parameters that govern the size and the shape of the hysteresis loop.

To obtain the Jiles-Atherton inverse model, equation (2d) needs to be replaced by the magnetization M partial derivative regarding the magnetic induction B. Based on the work of Sadowski et al. (2002) we have :

$$\frac{\partial M}{\partial B} = \frac{\eta}{\mu_0(k\delta - (\alpha - 1)\eta} \tag{3}$$

The conditions for the value of δ in (2i) must also change to depend on the variation of the magnetic induction B :

$$\delta = \begin{cases} +1 \text{ if } dB/dt > 0 \\ -1 \text{ if } dB/dt < 0 \end{cases} \tag{4}$$

By combining equations (2a), (2b), (2c), (3), (2e), (2f), (2g), (2h) and (4) we obtain the Jiles-Atherton inverse model.

In order to fit the hysteretic behavior of the LATM, the Particle Swarm Optimization (PSO), which is an evolutionary algorithm inspired on the paradigm of animal swarm intelligence and developed by Eberhart and Kennedy (1995), was used to find the optimal set of parameters for the inverse hysteresis model.
To minimize the maximum error of the inverse model, the experimental data used for fitting the model is the mean value of the dispersion range. As the dispersion range is $[0 - 50]$ mA, the fitting data for the inverse model is the 25 mA dispersion dataset.

3.3 Hysteresis Neural Network Inverse Model

At first, as the state of a hysteretic system depends on its history, parallel architecture Deep Neural Networks with Long-Short Term Memory (LSTM) and 1D Convolutional layers, for time series feature extraction, were used and gave excellent results for modelling hysteresis. Unfortu-

nately, the final Neural Network had to be downsized and architecture simplified due to :

- Hardware limitation : the RTM has limited memory storage, thus, the number of cells and hidden layers had to be reduced.
- Software limitation : the C code generation function, to embed the controller on the RTM, does not support every type of cells and parallel architecture networks.

Due to these constraints, the neural network has been limited to a single feedforward hidden layer with 128 cells, see Fig 4. The modelling performance of the Neural Network is degraded, but, as the complexity and size of the Neural Network can be compensated with an appropriate input vector (Kuczmannand Ivanyi, 2002), an appropriate choice of the inputs allowed getting a model with sufficient accuracy.
For the Neural Network to take into account the dependancy of the state's system to its history, it is fed with position at multiple time steps. The number of time steps was determined as the results of a trade-off : regression performance increases with the number of time steps as inputs but so does the Neural Network size. A compromise between Neural Network performance and its size was found by selecting 3 time steps which results in three inputs (θ_t, θ_{t-1}, and θ_{t-2}).
Also, when the input changes direction before reaching the maximum input value, it follows a First Order Reversal Curve (FORC) to reattach to the major loop. The FORC that is taken depends on the value of θ for which the signal has changed direction, θ_{inv}. This value is fed to the Neural Network.
Finally, the direction of the signal, θ_{dir}, is also given to the Neural Network.
The hidden and output layers cells' weights and bias make a regression between the input vector (θ_t, θ_{t-1}, θ_{t-2}, θ_{inv} and θ_{dir}) to determine the corresponding predicted current $\hat{i}_t$ to feed the LATM in order to achieve the desired position θ_t.

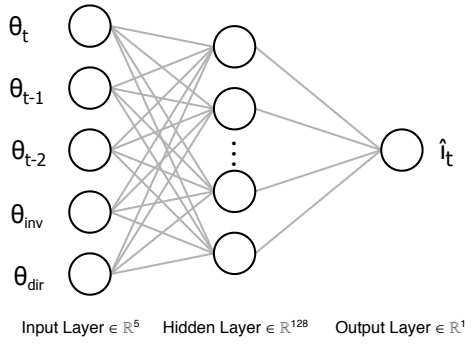

Fig. 4. Neural Network inverse model architecture

Neural Networks require a big amount of training data to give good regression results and the model needs to be efficient on any system in the dispersion range. Thus, the Neural Network could benefit from learning for the whole dispersion range to identify dispersion dependant features or avoid overfitting. The Neural Network was trained on the whole dispersion range of the hysteresis with a set of 2,750,000 data, 70% used for the training, 15% for testing and 15% for validation.

3.4 Inverse Modelling Performance

The Jiles-Atherton inverse model after parameter optimization and the Neural Network inverse model after training are given in Fig 5. The 25 mA dispersion dataset obtained experimentally and used for the Jiles-Atherton fitting is displayed for comparison.

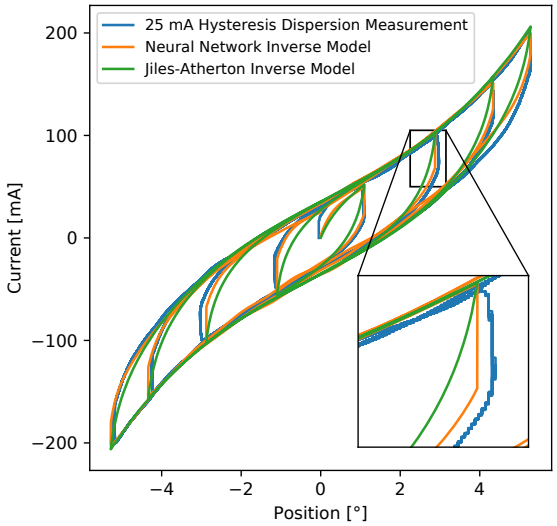

Fig. 5. Fitting of Neural Network and Jiles-Atherton inverse models, with local zoom

The result of the global optimization algorithm for the Jiles-Atherton model gives good results in terms of size and shape, see Fig 5, except on inversion points, where the slope discontinuity due to mathematical backlash has not be captured correctly.
Even if the Neural Network has been trained on the whole dispersion dataset and without external help, the obtained model fits the mean 25 mA dispersion dataset, see Fig 5. It even reproduces more precisely than the Jiles-Atherton inverse model the behavior of the system with a 25 mA dispersion. The slope discontinuity has been captured by the training.

4. CONTROL PERFORMANCE

The controller is now designed: the Jiles-Atherton inverse model parameters are optimized, the Neural Network inverse model is trained and the PI controller and AW parameters have been determined. In this section, the two controllers' performance will be evaluated with the following two tests : sinusoidal response, with varying magnitude and step response.
These two tests will be repeated on the whole dispersion range, 0 to 50 mA, every 5 mA and their reference signals are given in Fig 6.

4.1 Sinusoidal Response

In this section, the frequency response of the closed-loop will be tested with a varying magnitude sine wave for the following frequencies : 0.5 Hz, 1.0 Hz, 2.5 Hz, 5.0 Hz, and

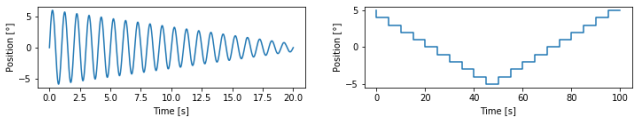

(a) Sinusoidal test ($1Hz$) (b) Step test

Fig. 6. Reference signals for tests

7.5 Hz. Fig 6a gives the reference signal θ_r for the test at 1.0 Hz.
The closed-loop behavior under a harmonic reference signal is given Fig 7. Fig 7a corresponds to the nominal case (a dispersion of 25 mA and a reference signal at 1.0 Hz), the linerization of the system is almost perfect. When the system moves away from the nominal case, the linearization is of course degraded, Fig 7b.

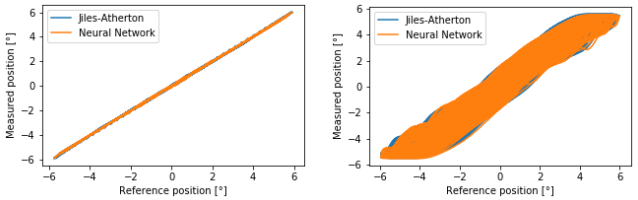

(a) 1.0 Hz reference signal (b) 5.0 Hz reference signal

Fig. 7. Linearization of the hysteretic system under a harmonic reference signal

A $10Hz$ sine wave was tested but the experiments with the Jiles-Atherton inverse model failed due to instability of the closed-loop when the dispersion was above 20 mA. This limitation was not encountered with the Neural Network based controller.
To evaluate the performance of the closed-loop control, the tracking error is calculated with the mean absolute error on position during the whole test :

$$\epsilon = \overline{|\theta_r - \theta|} \tag{5}$$

The results of the experiments are given in Fig 8. The top chart represents the log scale error, ϵ, depending on the emulated hysteresis dispersion for both models at each frequency while the bottom chart gives the relative error improvement, computed as the increase in accuracy obtained by the Neural Network controller compared to the Jiles-Atherton controller taken as reference.

Performance vs Dispersion
The dashed black line with triangle markers is the mean relative error improvement when taking the average over the 5 tested frequencies.
The Jiles-Atherton based controller error increases monotonically with dispersion despite the model being fitted for the 25 mA dispersion dataset. The Neural Network based controller finds its minimum error between 25 mA and 35 mA dispersion for low frequencies, 0.5 Hz and 1.0 Hz. At higher frequencies, 2.5 Hz, 5.0 Hz and 7.5 Hz, the errors follow the same trend as the Jiles-Atherton based controller, see Fig 8.
Overall, the artificial intelligence based controller improves the mean tracking error between 8% and 21% compared to the Jiles-Atherton based controller. This demonstrates the better robustness of the Neural Network model as the

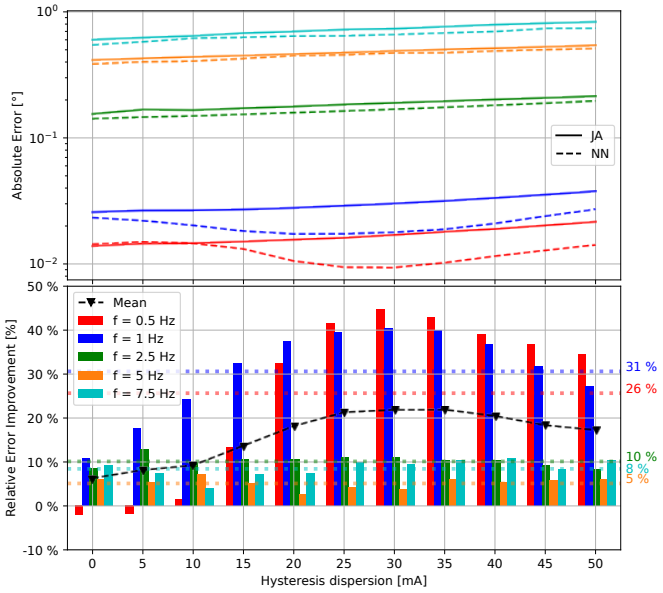

Fig. 8. Sine wave tracking error for both controllers depending on hysteresis dispersion

relative error improvement increases with dispersion up to 35 mA before slightly decreasing for low frequency. The relative error improvement decreases at stronger dispersion because the error is dispersion-mean centered.

Performance vs Frequency
Regardless of the model used by the controller, the error increases with frequency, see Fig 8 and Fig 7.
The Neural Network based controller has its best mean relative control performance (see colored dotted lines) at low frequencies $0.5Hz$ and $1.0Hz$, respectively 26% and 31%. It is less performant when the frequency rises, $2.5Hz$ and $5.0Hz$, as the relative performance improvement decreases, respectively 10% and 5%. At $7.5Hz$, the error improvement rises again to 8% as the Jiles-Atherton model performance falls off when getting closer to 10 Hz where it caused instability.

4.2 Step Response

In this section, the dynamic response of the system will be tested with steps. In addition to hysteresis variability, dispersion in the dynamic of the system has been emulated by changing the proportional gain of the controller. Three proportional gains have been tested : $0.5K_P$, K_P and $1.5K_P$.
To evaluate the closed-loop dynamic response relative improvement, two temporal criteria are considered, the 63% rising time and the overshoot in %, displayed respectively in Fig 9 and Fig 10.
To avoid observing the system's dynamic response at an unique operating point and to smooth out outliers, the two temporal criteria of the dynamic response will be computed as the average of the temporal criteria of the responses to the twenty steps of the reference signal given in Fig 6b. The different steps are maintained for 5 s to ensure the steady-state.

63% **Rising Time**
The improvement of the mean rising time of the closed-loop system with the Neural Network based controller is rather null when taking the nominal proportional gain of the controller, K_P (see the blue dotted line close to zero). The improvement is more significant, around 13%, for $0.5K_P$ and $1.5K_P$, that emulate the dispersion of the system dynamic, see Fig 9.
The overall faster rising time response of the closed-loop system can be explained by the models dynamics. The Neural Network converge faster to the steady state value than the Jiles-Atherton model as it does not have derivative and integral terms.

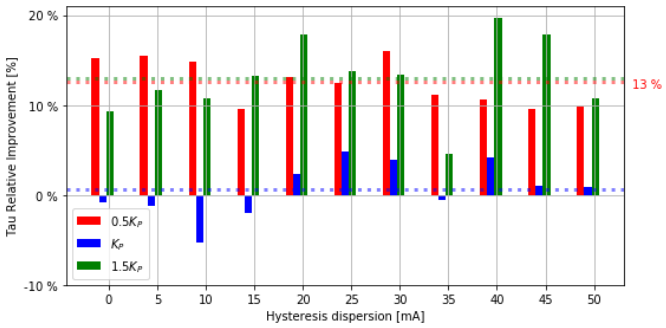

Fig. 9. Rising time relative improvement depending on hysteresis dispersion

Overshoot (%)
While the improvement is not significant with the nominal proportional gain, K_P, it can be noted that the mean overshoot is reduced by 5% and 16% with $0.5K_P$ and $1.5K_P$ (see the dotted lines).

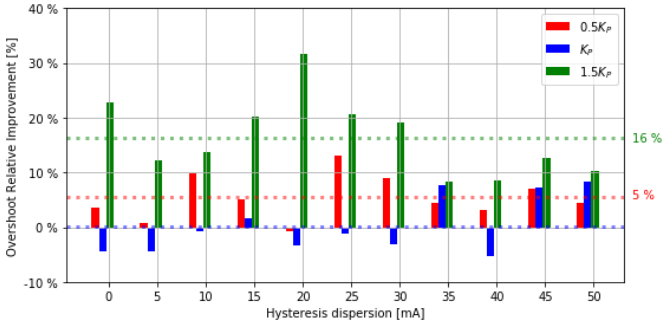

Fig. 10. Overshoot relative improvement depending on hysteresis dispersion

5. CONCLUSION

This paper has focused on modelling and controlling hysteresis for a highly dispersed system. System variability cannot be suppressed and taking it into account limits the performance of the conventional hysteresis compensation methods.
A control scheme based on a Neural Network inverse model of a hysteretic system has been computed and implemented on a dispersed system. To evaluate the robustness of the proposed control strategy, its performances were compared with a Jiles-Atherton inverse model based controller through two HIL tests : frequency and temporal responses.
The Neural Network based controller performed better in both tests showing also better robustness properties over the dispersion range. In average over the tested domain, the tracking error was improved by 8% and 21%, the rising time was enhanced up to 12% and the overshoot was reduced up to 18%.
These improvements can be explained by the overall better nonlinear fitting capabilities of artificial intelligence based models. They contain a larger number of parameters that gives the model a wider range of modelling capability.
In future works, the dependency of error to frequency could be further reduced by improving the robustness to frequency of the control algorithm.

ACKNOWLEDGEMENTS

The authors would like to acknowledge ISAE-SUPAERO and the French National Association of Research and Technology who participate in the funding of the PhD thesis.

REFERENCES

Al Janaideh, M., Rakheja, S., and Su, C.Y. (2009). Experimental characterization and modeling of rate-dependent hysteresis of a piezoceramic actuator. *Mechatronics*, 19(5), 656–670.
Chen, L., Feng, Y., Li, R., Chen, X., and Jiang, H. (2019). Jiles-atherton based hysteresis identification of shape memory alloy-actuating compliant mechanism via modified particle swarm optimization algorithm. *Complexity*, 2019.
Eberhart, R. and Kennedy, J. (1995). A new optimizer using particle swarm theory. In *MHS'95. Proceedings of the Sixth International Symposium on Micro Machine and Human Science*, 39–43. Ieee.
Hassani, V., Tjahjowidodo, T., and Do, T.N. (2014). A survey on hysteresis modeling, identification and control. *Mechanical systems and signal processing*, 49(1-2), 209–233.
Jiles, D. (2015). *Introduction to magnetism and magnetic materials*. CRC press.
Jiles, D.C. and Atherton, D.L. (1986). Theory of ferromagnetic hysteresis. *Journal of magnetism and magnetic materials*, 61(1-2), 48–60.
Joey, Z.G., Chang, L., and Pérez-Arancibia, N.O. (2019). Position control of a shape-memory alloy actuator using a preisach-model-based inverse-temperature method. In *2019 American Control Conference (ACC)*, 3801–3808. IEEE.
Li, Z. and Gong, Y. (2019). Research on ferromagnetic hysteresis of a magnetorheological fluid damper. *Frontiers in Materials*, 6, 111.
Liang, Y., Xu, S., Hong, K., Wang, G., and Zeng, T. (2019). Neural network modeling and single-neuron proportional–integral–derivative control for hysteresis in piezoelectric actuators. *Measurement and Control*, 0020294019866846.
Lu, H.l., Wen, X.s., Lan, L., An, Y.z., and Li, X.p. (2015). A self-adaptive genetic algorithm to estimate

ja model parameters considering minor loops. *Journal of Magnetism and Magnetic Materials*, 374, 502–507.

Nasiri-Zarandi, R., Mirsalim, M., and Cavagnino, A. (2015). Analysis, optimization, and prototyping of a brushless dc limited-angle torque-motor with segmented rotor pole tip structure. *IEEE Transactions on Industrial Electronics*, 62(8), 4985–4993.

Patel, M., Lal, S.K., Kavanagh, D., and Rossiter, P. (2011). Applying neural network analysis on heart rate variability data to assess driver fatigue. *Expert systems with Applications*, 38(6), 7235–7242.

Querlioz, D., Bichler, O., Dollfus, P., and Gamrat, C. (2013). Immunity to device variations in a spiking neural network with memristive nanodevices. *IEEE Transactions on Nanotechnology*, 12(3), 288–295.

Ramarotafika, R., Benabou, A., and Clénet, S. (2013). Stochastic jiles-atherton model accounting for soft magnetic material variability. *COMPEL: The International Journal for Computation and Mathematics in Electrical and Electronic Engineering*, 32(5), 1679–1691.

Rubežić, V., Lazović, L., and Jovanović, A. (2018). Parameter identification of jiles–atherton model using the chaotic optimization method. *COMPEL-The international journal for computation and mathematics in electrical and electronic engineering*, 37(6), 2067–2080.

Sadowski, N., Batistela, N., Bastos, J., and Lajoie-Mazenc, M. (2002). An inverse jiles-atherton model to take into account hysteresis in time-stepping finite-element calculations. *IEEE Transactions on Magnetics*, 38(2), 797–800.

Tan, Y., Dong, R., and He, H. (2019). Neural network based modeling of hysteresis in smart material based sensors. In *International Symposium on Neural Networks*, 162–172. Springer.

Tebble, R.S. and Craik, D.J. (1969). *Magnetic materials*, volume 455. Wiley-Interscience London.

Tsai, C.C., Lin, S.C., Huang, H.C., and Cheng, Y.M. (2009). Design and control of a brushless dc limited-angle torque motor with its application to fuel control of small-scale gas turbine engines. *Mechatronics*, 19(1), 29–41.

Yi, S., Yang, B., and Meng, G. (2019). Microvibration isolation by adaptive feedforward control with asymmetric hysteresis compensation. *Mechanical Systems and Signal Processing*, 114, 644–657.

Yu, Z.Y. and Wang, Z.Q. (2014). Analysis and simulation of a limited-angle torque motor. In *Applied Mechanics and Materials*, volume 668, 601–606. Trans Tech Publ.

Zhang, C., Jin, J., Na, W., Zhang, Q.J., and Yu, M. (2018). Multivalued neural network inverse modeling and applications to microwave filters. *IEEE Transactions on Microwave Theory and Techniques*, 66(8), 3781–3797.

Zhou, Y., Hu, J., Huang, Y., Li, X., and Zhu, X. (2019). Parameter identification and hysteresis compensation for piezoelectric stack based on bouc-wen model using genetic algorithm. In *2019 Chinese Control Conference (CCC)*, 313–317. IEEE.